


INFLUENCE OF MACHINE PARAMETERS ON THE PHYSICAL CHARACTERISTICS OF 3D-PRINTED SAND MOLDS FOR METAL CASTING

N. Bryant

Imerys S&T, Suwanee, GA, USA

T. Frush and J. Thiel

University of Northern Iowa, Cedar Falls, IA, USA

E. MacDonald and J. Walker 

Youngstown State University, Youngstown, OH, USA

Copyright © 2020 American Foundry Society
<https://doi.org/10.1007/s40962-020-00486-3>

Abstract

3D sand printing is an emerging technology that is enabling new possibilities in metal casting with respect to part complexity, casting design, and rapid mold production. The 3D printing technology, also known as additive manufacturing, is a binder jetting process which involves selectively depositing a furan-based binder into a sand bed one thin layer at a time. Over the course of the process, layers are subsequently added until the entire part has been fabricated. Although the use of 3D-printed sand molds in the foundry industry is growing, significant hesitation to widespread implementation remains. In this work, an investigation was conducted to determine the influence of machine settings on the physical characteristics of 3D-printed sand. Two factorial matrices were constructed to directly measure the significance of six settings that change

the resin content and compaction characteristics of the bonded sand. Factors include: X-resolution, printhead voltage, layer thickness, and the frequency, speed, and angle of the recoater blade. Responses include: density, permeability, strength, scratch hardness, loss on ignition, and print resolution. Several relationships are reported between machine settings and physical properties of the product. These results will help inform mold manufacturing as the foundry industry continues to adopt additive technologies.

Keywords: metal casting, 3D printing, additive manufacturing, binder jetting, process development

Introduction

Recent developments in additive manufacturing (AM) are revolutionizing the foundry industry's capability to create molds and cores.^{1,2} Using binding jetting AM technology, sand molds and cores can be rapidly fabricated directly from a computer-aided design (CAD) model.³ AM metal casting tooling is catalyzing a dramatic shift in the design philosophy from techniques that are, in some cases, thousands of years old. Direct fabrication of mold components via AM, also known as 3D printing, has increased the design freedom for metal castings and greatly accelerated the pace of prototyping compared to traditional methods.⁴⁻⁶ High tooling costs and long lead times are often associated with the metal casting process.⁷ With direct

production of molds and cores via 3D sand printing, though, hard tooling is completely eliminated from the manufacturing process. This significantly reduces the time and cost from initial design to the production of a casting.

However, 3D sand printing is still in the early stages of evolution and currently transforming from a low-volume and prototype market to production levels. Recent and rapid technological advancements, which are further increasing the process efficiency, are enabling this transformation. Historically, owners of additive manufacturing machines were often constrained to use limited materials provided from the manufacturer of the equipment to ensure quality prints.

Several investigations have been conducted that study the viability of commercial aggregates in these machines.^{2,8} Other researchers have focused on the material systems themselves including binder burnout characteristics⁹ and thermal expansion properties of chemically bonded silica sand.¹⁰ The effect of 3D-printed molds on casting mechanical properties¹¹ and casting surface finish¹² has also been reported in the literature. Other noteworthy research on 3D-printed sand molds includes process modeling,¹³ in situ process monitoring for data acquisition, quality control and verification,^{14–16} and the development of lightweight cellular structures and composite materials.^{17,18}

Despite the growing body of research and demonstrated success in production of 3D-printed sand molds, there remains uncertainty surrounding the technology within the industry. High capital costs and unknown mold properties serve as barriers to many potential adopters. In this work, the effect of 3D printing process parameters on sand mold properties is systematically and comprehensively investigated. It is shown that a wide array of mold characteristics can be modulated with proper understanding and control of machine parameters. Therefore, the twenty-first-century foundryman can not only rely on 3D-printed sand molds but optimize mold characteristics (e.g., tailoring mold strength, permeability, or resolution) depending on casting requirements.

3D Sand Printing

The sand printing process can be divided into three separate steps: mixing, layering, and printing. The first step, mixing, is performed by homogenizing a specified level of acid catalyst with a set quantity of sand. In this work—and indeed in nearly all 3D sand printers—the organic furan resin system is used. Furan systems are widely known in the casting industry as they were used extensively in the 1970s and 1990s due to their combination of high strength and favorable shakeout characteristics. This step is often completed automatically within an onboard mixing chamber incorporated on the machine. Once the materials are sufficiently mixed, the resultant coated sand grains are deposited into a recoater, which is a component that deposits the sand layer. Once the recoater is full of pre-activated sand (i.e., mixed with acid catalyst), the build platform lowers by a distance of one layer thickness. Subsequently, the recoater distributes a layer of sand in the allotted space. Lastly, a printhead moves across the build area and fires droplets of furan resin in regions specified by the CAD model. This process is repeated until all the individual cross-sectional images of the 3D CAD model have been successfully printed, upon which the finished part can be excavated from the build box.

Sand printing machines have a multitude of settings that can be changed to influence the physical properties of the resultant parts, as illustrated within recipe editor (Figure 1) of the ExOne S-Max 3D sand printer. An experienced operator is more likely to understand both the overall influence of process parameters and jargon present in this interface; however, this is generally due to increased operation experience over time, rather than a sophisticated training protocol. In other words, there are scarce information and documentation that inform new operators and machine purchasers about the influence of these parameters. This investigation intends to enlighten the industry with information about some of the most important settings the machine purchaser is likely to experiment with when standardizing the operation.

X-Resolution

The X-resolution, which is provided in units of distance, changes the spacing between individual droplets of resin when the printhead fires. Here, decreasing the X-resolution distance allows more droplets of resin to be placed over across a unit length. Therefore, this setting is often adjusted to change the strength characteristics of the printed parts as well as controlling loss on ignition.

Furthermore, the print speed, a separate variable, is strictly dependent on the X-resolution. This is because the printhead cannot closely eject droplets accurately if it is moving with excessive velocity. It is common practice to change the print speed to the highest allowable velocity for a specified X-resolution, which the machine automatically calculates during the adjustment period.

Layer Thickness

Layer thickness, also referred to as the Z-resolution, changes the magnitude of the distance that the build platform is lowered after each print cycle. This setting directly affects how many layers are required to build a specified geometry—a balance between time efficiency and part quality. A smaller layer thickness increases resolution by minimizing stair step size and increases the resin content of the printed part due to increasing the number of printhead passes that occur. However, these come at the cost of significantly increasing build time and therefore lowering manufacturing efficiency.

Printhead Voltage

Most printhead technology in sand printers is piezoelectric in nature. The technology works when a driving voltage is applied to a piezotransducer, upon which the piezoelectric element rapidly transitions between a swelling and

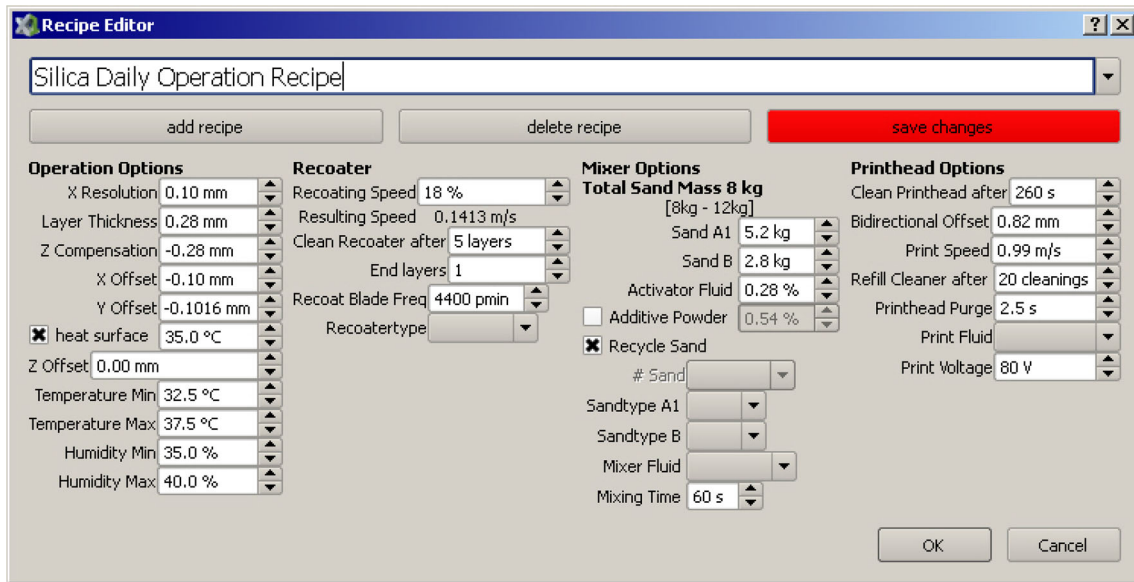


Figure 1. Recipe editor from the S-Max 3D sand printer.

contracting action. This causes the element to displace an amount of liquid contained within the printhead, ejecting it as a droplet onto the build area.¹⁹ The printhead voltage directly changes the amplitude of the waveform curve, an example of which is shown in Figure 2.

Here, T_{rise} is the time required for the printhead voltage to be applied to the piezoelectric element, T_{dwell} is the time that voltage is sustained, and T_{fall} is the time required for the voltage to dissipate. When the voltage amplitude increases, the element displacement during the sustainment period of the waveform similarly increases. Thus, the pressurization and subsequent droplet inertia increase as well. Liou et al.²⁰ demonstrated the relationship between increasing voltage and increasing droplet size and detailed issues related to satellite droplet formation at exceedingly high voltages.

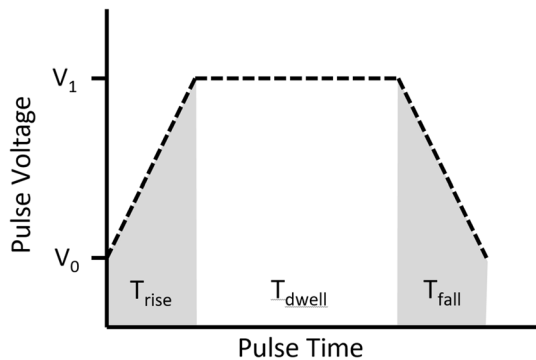


Figure 2. A theoretical waveform curve for a piezoelectric printhead.

Recoater Blade Oscillation

The recoater component is loaded with an oscillating blade that is used to compact the pre-activated sand grains during layer deposition. The frequency at which the oscillation cycle is completed can be adjusted, which has an effect on the printed sand density and permeability.

The recoater speed is often changed in conjunction with the recoater blade frequency, because they directly interact with each other. Increasing the speed lowers the amount of time the oscillating blade has to compact the grains, and vice versa. While the recoater speed variable is expressed as a percentage in the recipe editor, the speed is supplied in meters per second as well. This can be used to calculate the total time it takes for the layer to be distributed. If this value of time is used in a calculation with the blade frequency, supplied in units of oscillations per minute, a more descriptive quantification is derived, namely oscillations per cycle (OPC).

$$OPC = \frac{\left(\frac{W}{v}\right)}{60} * \Omega$$

where v is the recoater speed in meters per second, W is the width of the build platform in meters, and Ω is the recoater frequency in oscillations per minute.

Recoater Blade Angle

The recoater angle is not a setting that is changed within the recipe editor interface, but rather through a mechanical manipulation of the recoater component itself. The oscillating blade is controlled by several eccentric bearings that cause the oscillation to occur by a range of $\pm 0.2^\circ$, and if the median angle is steepened, a more significant

compaction level is achieved, directly influencing the printed sand density and permeability similarly to the other recoater settings. A schematic representation of the steepening of the recoater angle is presented in Figure 3 (not to scale). It is shown that the oscillation range between the two examples is identical but the depth of the oscillation cycle has become more aggressive.

Testing Methods

Factorial Design

Two testing matrices were developed to interrogate the influence of machine printing parameters on the physical properties of additively manufactured sand. These matrices closely resemble a classic high/low factorial design of experiments, with each matrix consisting of eight individual testing series. The first of the two matrices is focused primarily on settings that impact the resin content of the sand and is displayed in Table 1. The three parameters investigated include the printhead voltage, X-resolution, and layer thickness.

The second factorial matrix, described in Table 2, was created to investigate the effect of recoater parameters on the bonded sand physical properties. As seen in the table, the recoater blade frequency, speed, and median angle were the parameters of interest in this portion of the investigation. Similar to the prior matrix, the representative values for the addition and subtraction symbols are given.

Sample Fabrication

Utilizing the settings provided from the matrices in the ExOne S-Max 3D sand printer, ten transverse specimens were manufactured in each series using a commercial 80 AFS-GFN silica to test several bonded sand characteristics including the printed sand density, permeability, transverse strength, scratch hardness, and loss on ignition. The transverse specimen is a standardized rectangular prism geometry with dimensions $8'' \times 1'' \times 1''$ ($203.2 \text{ mm} \times 25.4 \text{ mm} \times 25.4 \text{ mm}$). After ten measurements of each test, the average value was calculated with exception for

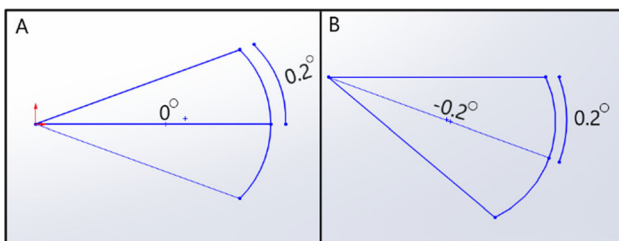


Figure 3. A schematic illustration of the oscillation cycle and its relation to the recoater angle: (a) baseline median angle of 0° , (b) adjusted median angle of -0.2° .

Table 1. The Resin Content Factorial Matrix

Series	Main effects		
	Voltage (V)	X-resolution (B)	Z-thickness (C)
1	–	–	–
2	+	–	–
3	–	+	–
4	+	+	–
5	–	–	+
6	+	–	+
7	–	+	+
8	+	+	+

Variables	Voltage (V)	X-resolution (mm)	Z thickness (mm)
+	85	0.20	0.42
–	76	0.14	0.28

Table 2. The Recoater Settings Factorial Matrix

Series	Main effects		
	Frequency (A)	Speed (B)	Angle (C)
1	–	–	–
2	+	–	–
3	–	+	–
4	+	+	–
5	–	–	+
6	+	–	+
7	–	+	+
8	+	+	+

Variables	Frequency (pmin)	Speed (%)	Median angle ($^\circ$)
+	4400	25	0
–	3600	15	-0.2

the loss on ignition, which was determined by the average of three samples.

Characterization

The printed sand density was determined by using a balance accurate to the tenth decimal place to determine the specimen mass in conjunction with a calibrated height gauge to measure the dimensions of each face of the bar to the thousandths decimal place. Using the measured data, the density was subsequently calculated for each series.

Bonded sand permeability was measured using a Dietert model 338 electric permimeter with a mold permeability attachment using the AFS 5223-05-S method.

The transverse strength was measured using a Simpson universal sand strength machine set to the core transverse strength setting. Once the machine sectioned each bar in half, the value on the display was recorded.

The scratch hardness was measured using a Simpson digital scratch hardness tester, which quantitatively describes the specimen's overall resistance to friability. After placing the device on the "Z" face of the bar, three complete rotations of the wheel were executed, which agrees with the methodology provided by the equipment manufacturer.

Loss on ignition for each series was determined according to the AFS 5100-12-S. Since the furan binder system used to adhere the sand grains is a thermoset polymer, upon reaching complete pyrolysis the total resin percentage can be calculated according to the change in weight.

Lastly, a methodology was developed to quantify the resolution of printed sand when various printing parameters are manipulated. Resolution in this case is defined according to the feature size that the printer is capable of creating, and it is divided into two criteria: cavities and protrusions. A new test specimen was fabricated to measure resolution and is shown in Figure 4 (left). This geometry, which will be referred to as an artifact, has both cavities and protrusions present within the model. Numbers were negatively extruded into the surface which correspond to the features used for measurement. A protruding cylinder, a cylindrical cavity, and a central space that align with the numbers on the model exhibit a dimension

(diameter or length) of exactly half the associated number in millimeters. For example, the cylindrical protrusion that aligns with the "8" on the artifact has a measured diameter of 8.0 mm.

When this geometry is printed, the machine will discard or fail to print some of the minute features on the artifact. Therefore, when the specimen was evaluated, the minimum feature size that is present on the geometry was used to quantify the resolution. Individual ratings were applied to each of the three features. In Figure 4 (right), the arrows indicate that this additively manufactured example artifact possesses a protrusion rating of 3, a gap rating of 2, and a cavity rating of 3, since their respective features correspond to the number present on the geometry, as previously discussed.

Results and Discussion

For all results generated from the matrix data, the error bars represent one measured standard deviation from the average of the respective bonded sand property.

Matrix 1: Resin Content

As shown in Figure 5, layer thickness was found to be the most critical factor influencing printed sand density, while the printhead voltage and X-resolution showed a fairly negligible, yet measureable difference between series samples. In this case, it is observed that the most dense samples were created from series 1, and the least dense samples were measured from series 7.

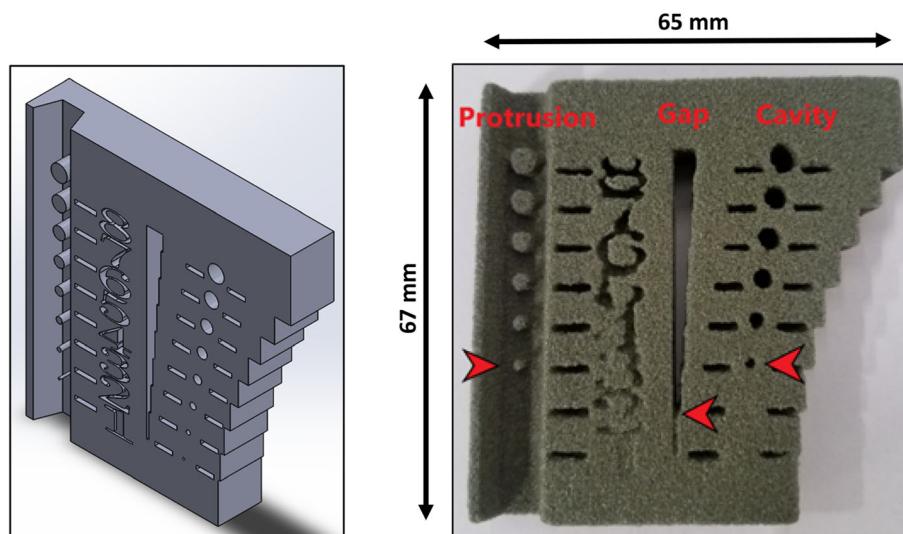


Figure 4. Left: CAD model of the artifact geometry used to measure printed sand resolution. Right: an example of a sand printed artifact that indicates how resolution was measured.

Printed Sand Density of 3D Printed Specimens from Matrix
1 - Resin Content

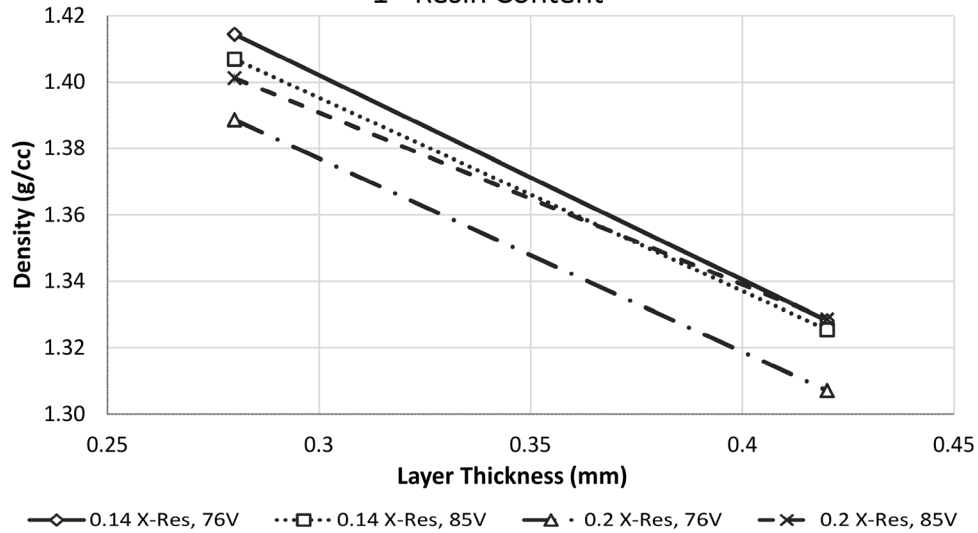


Figure 5. Results for printed sand density of 3D-printed specimens from the resin content matrix.

Permeability of 3D Printed Specimens from Matrix 1 -
Resin Content

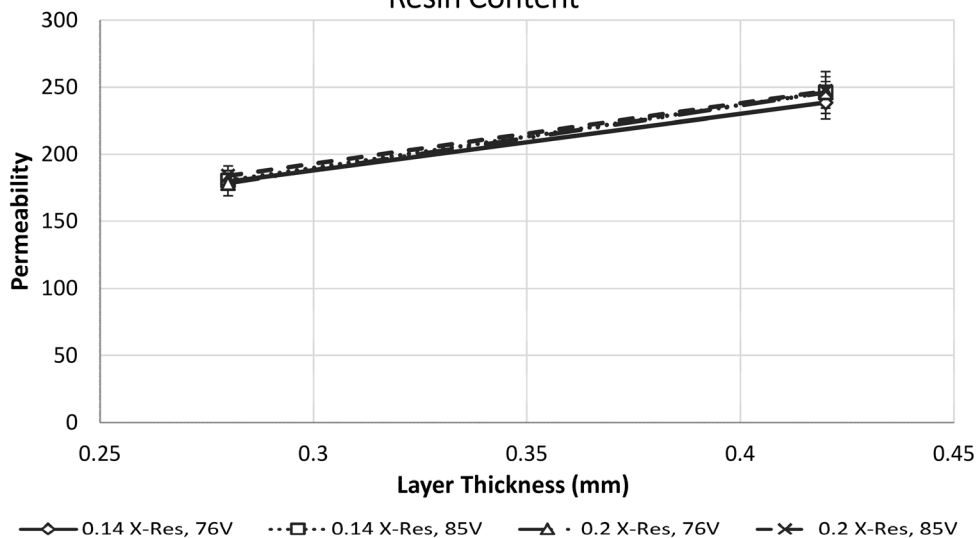


Figure 6. Results for permeability of 3D-printed specimens from the resin content matrix.

The permeability results, displayed in Figure 6, indicate that both printhead voltage and X-resolution have an insignificant influence on permeability. On the contrary, the layer thickness did exhibit a positive correlation with permeability, possibly due to the fact that by increasing layer thickness (and consequently lowering the quantity of print cycles per unit height) there were less compaction cycles performed by the recoater. These data are further supported by the printed sand density result discussed prior, because density and permeability generally have a negatively correlated relationship.

The transverse strength results from the resin content matrix are provided in Figure 7. As observed, the combination with the highest measured strength was series 1, and the lowest was series 7. The explanatory variable in this case was the layer thickness, which showed a consistent inverse relationship with transverse strength for all samples. The printhead voltage and x-resolution appeared to translate the function to different positions on the plot, with the lower X-resolutions residing on the higher y-positions and the higher X-resolutions exhibiting the opposite trend. Higher printhead voltages appeared to decrease the

Transverse Strength of 3D Printed Specimens from Matrix 1 - Resin Content

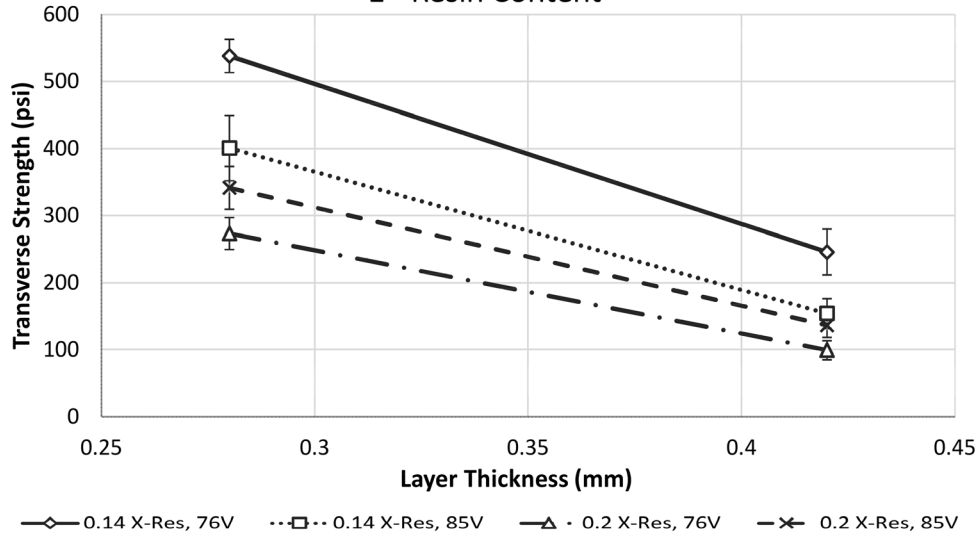


Figure 7. Results for transverse strength of 3D-printed specimens from the resin content matrix.

difference in transverse strength when the X-resolution was changed.

A unique result from the scratch hardness measurements is observed in Figure 8. The samples with 0.28 mm layer thickness did not show a significant difference in scratch hardness despite the changes in X-resolution and printhead voltage. However, an interaction effect is shown between high layer thickness (0.42 mm) and low X-resolution (0.14), where the printhead voltage has a significant affect.

Lastly, the loss-on-ignition results from the resin content matrix are displayed in Figure 9. There were a few expected observations that were measured, namely that increasing the layer thickness drastically reduced the loss on ignition. This was observed by with lower X-resolution (0.14 mm) resulting in higher loss on ignition than higher X-resolution (0.2 mm). However, a somewhat conflicting result is seen when printhead voltage is taken into consideration. For the series with X-resolution set to 0.2 mm, the sample produced by 85 V had a slightly higher resin content than the 76 V sample, but the opposite case is observed for the 0.14 X-resolution samples.

Scratch Hardness of 3D Printed Specimens from Matrix 1 - Resin Content

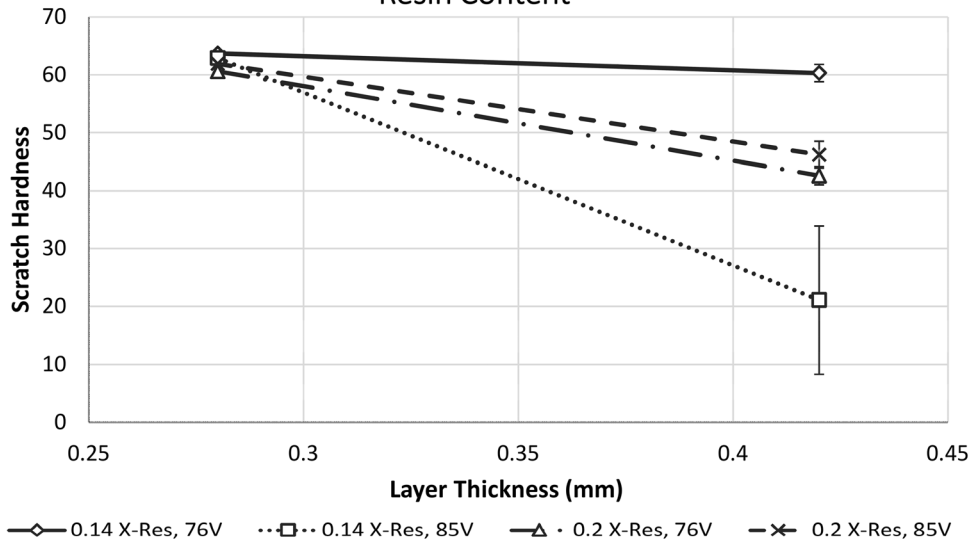


Figure 8. Results for scratch hardness of 3D-printed specimens from the resin content matrix.

Loss on Ignition of 3D Printed Specimens from Matrix 1 - Resin Content

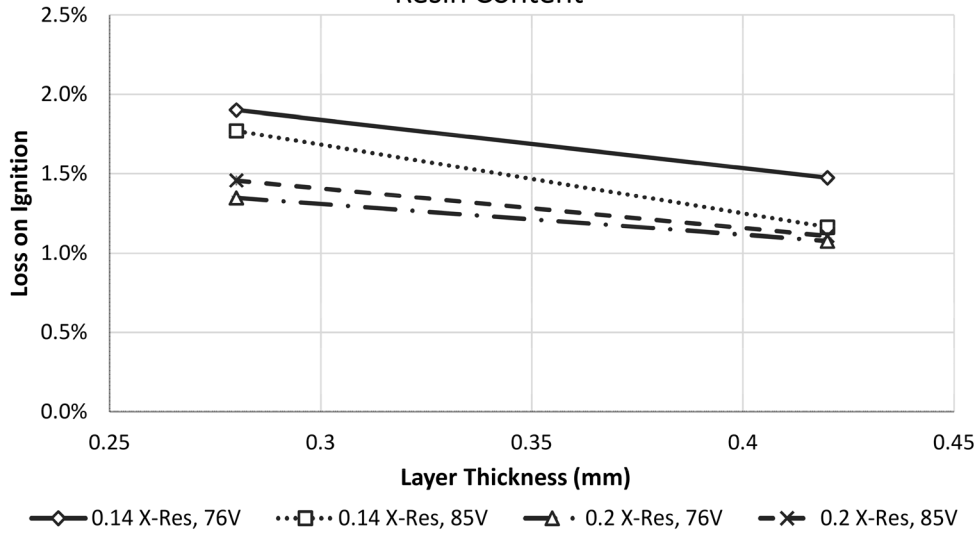


Figure 9. Results for loss on ignition of 3D-printed specimens from the resin content matrix.

Matrix 2: Recoater Settings

The results for all properties in the second matrix will be supplied as a function of oscillations per cycle according to Eqn. 1. Additionally, the different series in each chart represents the mechanical change of the recoater angle.

As presented in Figure 10, the printed sand density expressed a strong, linear relationship with oscillations per cycle. An increase in density is also observed according to the translation of the series by changing the recoater angle. In this case, steepening the median angle by -0.2° caused

a noticeable change in density, but by a factor lower than what was observed from the layer thickness in Figure 5. As hypothesized, the densest samples were created from series 2 with higher frequency, lower speed, and a steeper recoater angle. In contrast, the least dense samples were obtained from series 7, which had lower frequency, higher speed, and the base recoater angle.

With a change in printed sand density observed between series, a corresponding change in permeability was also measured for this matrix. This result is presented in Figure 11. Series 7 had the lowest permeability of all samples

Printed Sand Density of 3D Printed Specimens from Matrix 2 - Recoater Settings

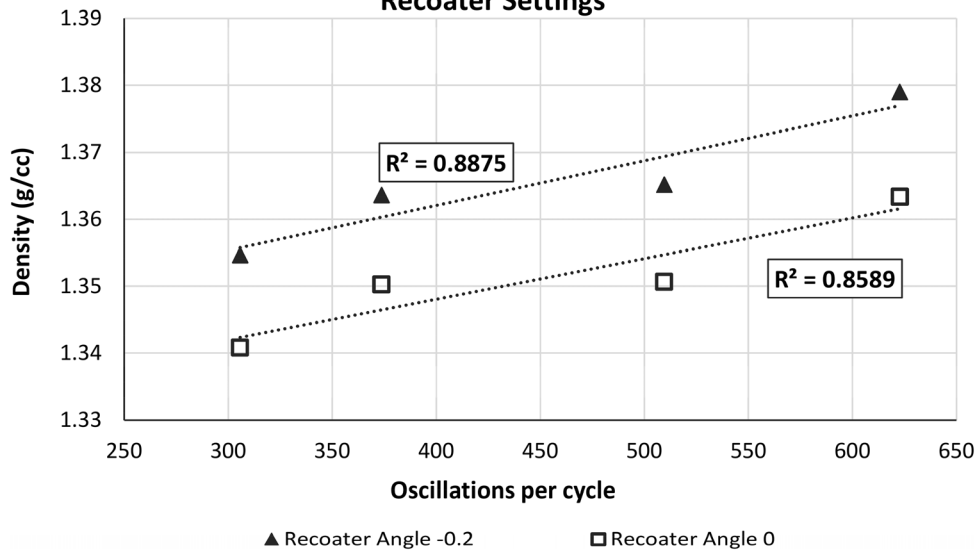


Figure 10. Results for printed sand density of 3D-printed specimens from the recoater settings matrix.

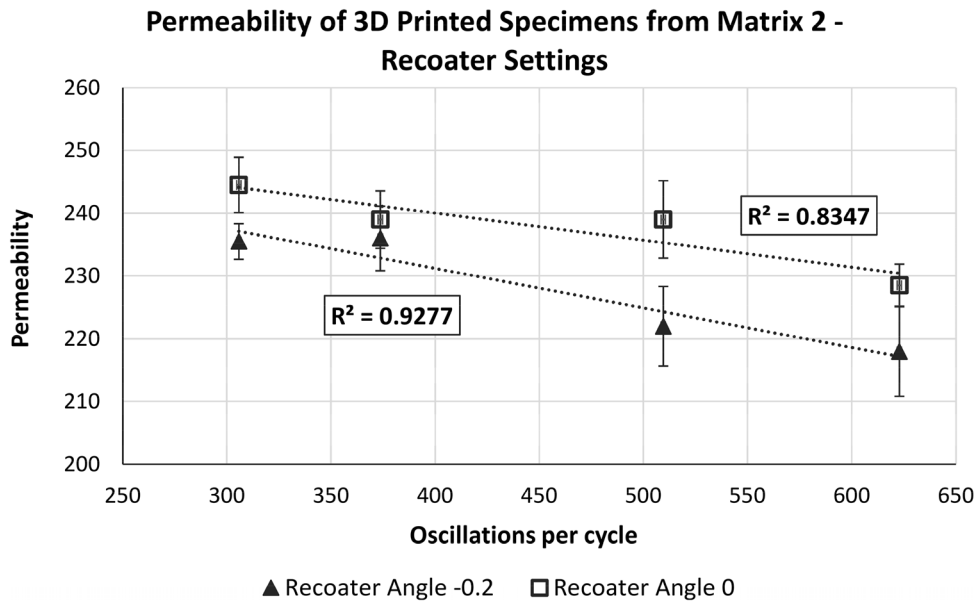


Figure 11. Results for permeability of 3D-printed specimens from the recoater settings matrix.

in this matrix, and series 2 showed the highest permeability. This was the opposite of the trend seen in the prior result for density, as expected.

It was originally thought that the change in density caused by manipulating the recoater settings would also influence the transverse strength of the product. However, as shown in Figure 12, there was not a significant difference measured between the samples, despite the quantity of oscillations per cycle doubling in some cases.

A similar result was also obtained from the scratch hardness data in Figure 13. The figure shows that the scratch hardness remained quite constant throughout the changes in settings, and there was significant overlap in the measured error, possibly indicating that the recoater angle also played an insignificant role.

Oscillations per cycle was also not a strong explanatory variable for loss on ignition, as seen by the measured data in Figure 14. In this matrix, there was no repeatable trend observed between samples, even though the individual points were quite isolated on the plot.

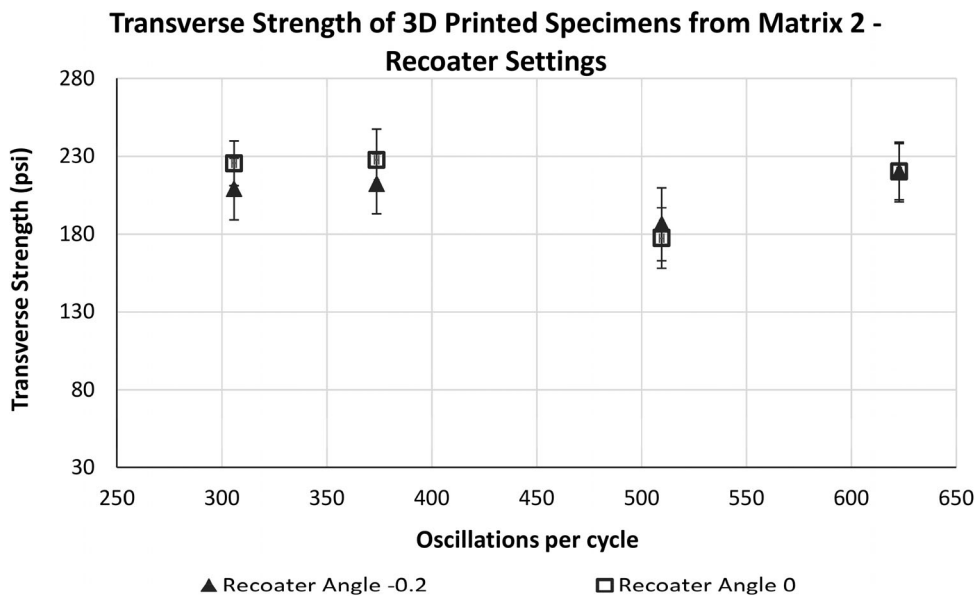


Figure 12. Results for transverse strength of 3D-printed specimens from the recoater settings matrix.

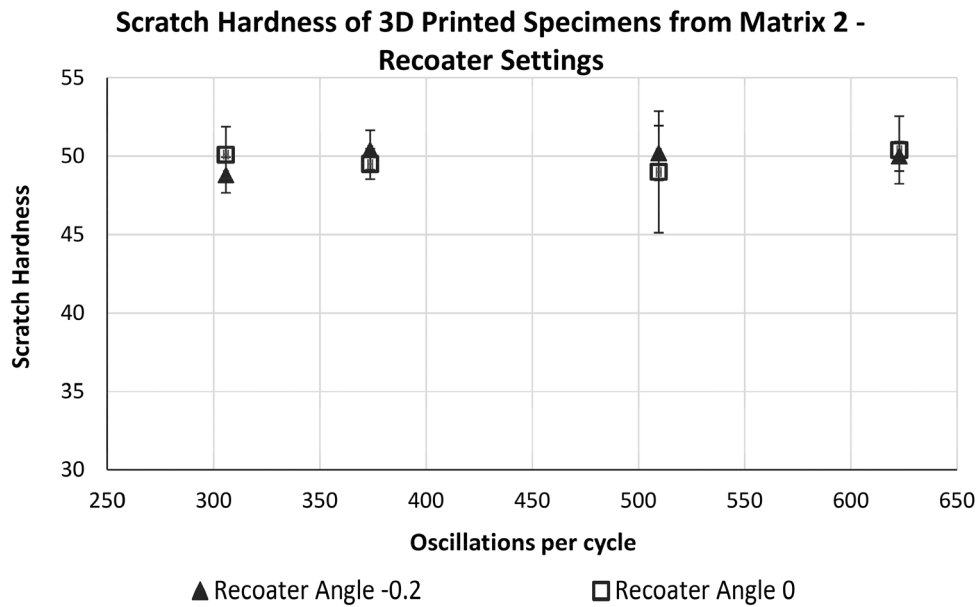


Figure 13. Results for scratch hardness of 3D-printed specimens from the recoater settings matrix.

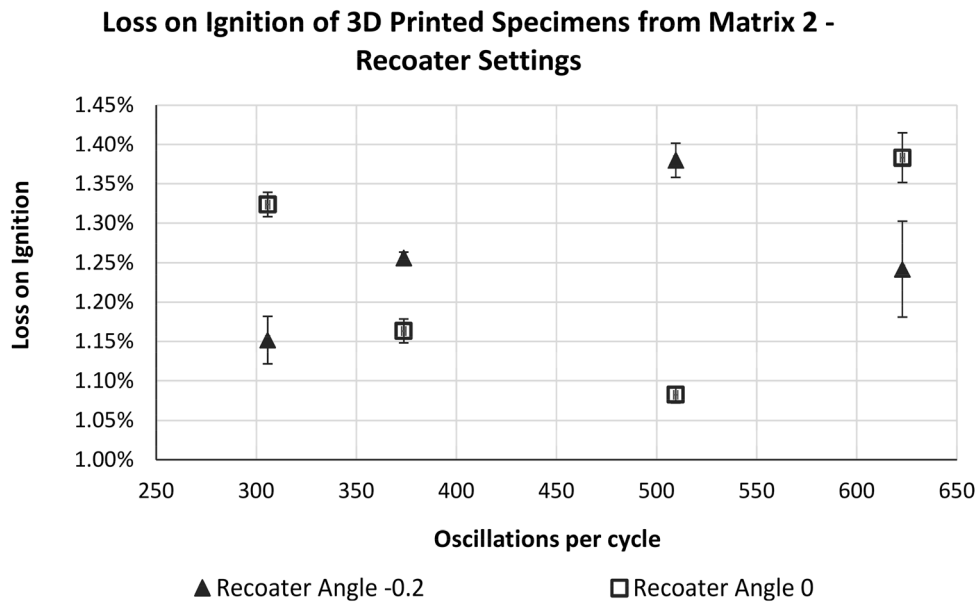


Figure 14. Results for loss on ignition of 3D-printed specimens from the recoater settings matrix.

Print Resolution

The resolution data measured from the 3D-printed artifact geometry are presented in Figure 15. Here, lower Resolution Rating scores are indicative of higher resolution. The most influenced parameter was the cavity resolution, which appeared to improve significantly when the loss on ignition decreased. Contrary to that relationship, the protrusion rating degraded slightly at lower relationships. The gap resolution remained constant throughout all series.

In this case of the second matrix, recoater settings did not appear to influence the resolution measured from the artifacts, as observed in Figure 16. The cavity resolution was nearly constant between all samples. This occurred despite the large variation in oscillations per cycle. The gap resolution also remained constant, similarly to the prior figure. Lastly, the protrusion rating was the most impacted in this portion of the investigation, but it did not follow a repeatable trend with the oscillations per cycle. This change could be attributed to normal variation.

Resolution Measurements of 3D Printed Specimens from Matrix 1
- Resin Content

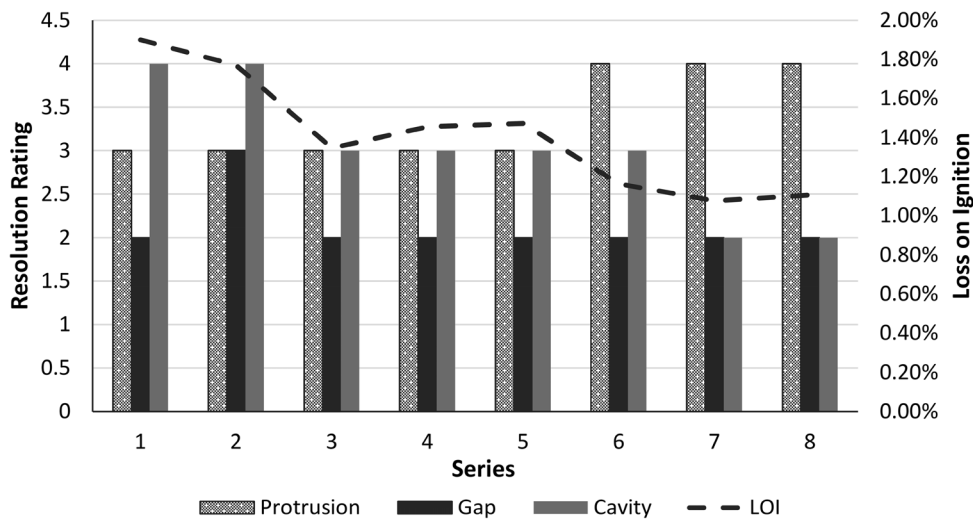


Figure 15. Results for resolution obtained from 3D-printed artifact geometry for the resin content matrix.

Resolution Measurements of 3D Printed Specimens from Matrix 2
- Recoater Settings

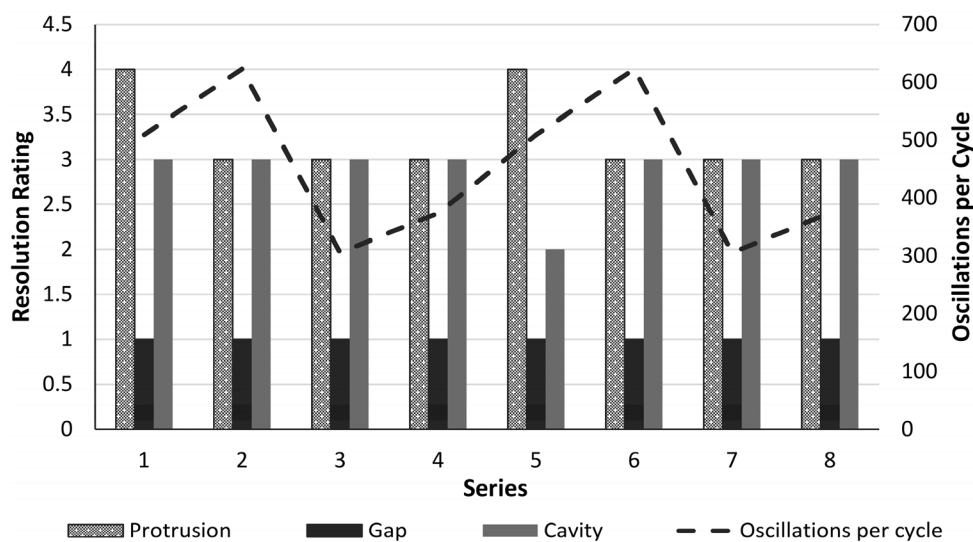


Figure 16. Results for resolution obtained from 3D-printed artifact geometry for the recoater settings matrix.

Conclusion

The results indicate that there are wide varieties of parameters that influence the characteristics of 3D-printed sand. It was determined that settings that directly influence the resin content of the product heavily influence the transverse strength, loss on ignition, printed sand density, and resolution with a repeatable trend. In the case of the recoater settings, the oscillations per cycle quantification offered a strong explanatory variable for printed sand density and permeability. The scratch hardness was the

only investigated parameter that did not exhibit a repeatable trend with the covariates.

The relationships obtained from this investigation can be used to help new machine purchasers maintain process control within the operation, as desirable properties can be achieved by manipulating the investigated settings. However, it should be noted that the properties of the product would change over time due to the inevitable degradation of the machine components even if no settings were changed. Therefore, an understanding of the machine settings on mold characteristics as evidenced in this work will

facilitate adjustments during the lifetime of the machine to maintain consistent quality. Furthermore, not all molds and castings are created equal. In some cases, such as castings that require thin or filigree core components, high mold strength is desirable to maintain the integrity of printed component during cleaning, shipping, assembling, and casting. In other cases with simple but large mold geometries, increased permeability may be necessary to facilitate gas escape while strength can be conceded. It is important for the casting engineer and the machine operator to understand the influence of machine parameters on mold characteristics—and the compromises involved—to produce the highest quality molds and castings.

Acknowledgements

This effort was performed through the National Center for Defense Manufacturing and Machining under the America Makes Program entitled “Maturation of Advanced Manufacturing for Low Cost Sustainment (MAMLS)—Additional Work for Research Project #1, Phase 1” and is based on research sponsored by Air Force Research Laboratory under Agreement Number FA8650-16-2-5700.

REFERENCES

1. R. Singh, Three dimensional printing for casting applications: a state of art review and future perspectives. In *Advanced materials research 2010* (Vol. 83, pp. 342–349). Trans Tech Publications
2. J. Thiel, S. Ravi, N. Bryant, Advancements in materials for three-dimensional printing of molds and cores. *Inter. Metalcast.* **11**, 3–13 (2017). <https://doi.org/10.1007/s40962-016-0082-y>
3. P. Beeley, *Foundry Technology* (Elsevier, 2001)
4. E.M. Sachs, Three dimensional printing techniques. United States Patent No. 5204055 (1993)
5. E. Sachs, M. Cima, J. Cornie, D. Brancazio, J. Brecht, A. Curodeau, M. Esterman, T. Fan, C. Harris, K. Kremmin, S.J. Lee, Dimensional printing: rapid tooling and prototypes directly from CAD representation. In *International Solid Freeform Fabrication Symposium*, Austin, TX 1990 (pp. 27–47)
6. D. Bak, Rapid prototyping or rapid production? 3D printing processes move industry towards the latter. *Assem. Autom.* **23**(4), 340–345 (2003)
7. C.W. Lee, C.K. Chua, C.M. Cheah, L.H. Tan, C. Feng, Rapid investment casting: direct and indirect approaches via fused deposition modelling. *Int. J. Adv. Manuf. Technol.* **23**(1–2), 93–101 (2004)
8. K. Woods, Sand distribution effect on three dimensional printed sand properties (2018). *Electronic theses and dissertations.* 534
9. D. Snelling, C. Williams, A. Druschitz, A comparison of binder burnout and mechanical characteristics of printed and chemically bonded sand molds. In *SFF Symposium*, Austin, TX (2014)
10. J. Thiel, Thermal expansion of chemically bonded silica sand. *AFS Trans.* **119**, 369–378 (2011)
11. D. Snelling, C. Williams, A. Druschitz, Mechanical and Material Properties of Castings produced via 3d printed molds. *Addit. Manuf.* (2019)
12. E. Bassoli, A. Gatto, L. Iuliano, Violante M. Grazia, 3D printing technique applied to rapid casting. *Rapid Prototyp. J.* **13**(3), 148–155 (2007)
13. H. Miyanaji, S. Zhang, L. Yang, A new physics-based model for equilibrium saturation determination in binder jetting additive manufacturing process. *Int. J. Mach. Tools Manuf.* **124**, 1 (2018)
14. J. Walker, E. Harris, C. Lynagh, A. Beck, R. Lonardo, B. Vuksanovich, J. Thiel, K. Rogers, B. Conner, E. MacDonald, 3D printed smart molds for sand casting. *Inter. Metalcast.* **12**, 785–796 (2018). <https://doi.org/10.1007/s40962-018-0211-x>
15. J.M. Walker, A. Prokop, C. Lynagh, B. Vuksanovich, B. Conner, K. Rogers, J. Thiel, E. MacDonald, Real-time process monitoring of core shifts during metal casting with wireless sensing and 3D sand printing. *Addit. Manuf.* **27**, 54–60 (2019)
16. J. Kobliska, P. Ostojic, X. Cheng, X. Zhang, H. Choi, Y. Yang, X. Li, Rapid fabrication of smart tooling with embedded sensors by casting in molds made by three dimensional printing. In *Proc. of Solid Freeform Fabrication Symposium 2005* (pp. 468–475)
17. D. Snelling, H. Blount, C. Forman, K. Ramsburg, A. Wentzel, C. Williams, A. Druschitz, The effects of 3D printed molds on metal castings. In *Proceedings of the Solid Freeform Fabrication Symposium 2013* (pp. 827–845)
18. D. Snelling, Q. Li, N. Meisel, C.B. Williams, R.C. Batra, A.P. Druschitz, Lightweight metal cellular structures fabricated via 3D printing of sand cast molds. *Adv. Eng. Mater.* **17**(7), 923–932 (2015)
19. Y.F. Liu, M.H. Tsai, Y.F. Pai, W.S. Hwang, Control of droplet formation by operating waveform for inks with various viscosities in piezoelectric inkjet printing. *Appl. Phys. A* **111**(2), 509–516 (2013)
20. T.M. Liou, C.Y. Chan, K.C. Shih, Effects of actuating waveform, ink property, and nozzle size on piezoelectrically driven inkjet droplets. *Microfluid. Nanofluid.* **8**(5), 575–586 (2010)

Publisher’s Note Springer Nature remains neutral with regard to jurisdictional claims in published maps and institutional affiliations.